Journal of Electronic Materials (2022) 51:4152–4160
https://doi.org/10.1007/s11664-022-09731-3

TOPICAL COLLECTION: SYNTHESIS AND ADVANCED CHARACTERIZATION OF MAGNETIC OXIDES

Influence of Co-In Doping in *M*-Type Barium–Strontium Hexagonal Ferrite on Microwave Absorption

Harsimrat Kaur[1] · K. S. Bhatia[2] · B. S. Tewari[3] · P. Mandal[4] · A. Dhyani[4]

Received: 3 February 2022 / Accepted: 23 May 2022 / Published online: 13 June 2022

Abstract

The present paper deals with the study of microwave absorption properties of cobalt- and indium-doped *M*-type barium–strontium ($Ba_{0.5}Sr_{0.5}Co_xIn_xFe_{12-2x}O_{19}$) hexagonal ferrites. The standard ceramic method is used to synthesize $Ba_{0.5}Sr_{0.5}Co_xIn_xFe_{12-2x}O_{19}$ hexagonal ferrite of varying compositions ($x = 0.0, 0.2, 0.4, 0.6, 0.8, 1.0$) sintered at 1100°C for pellet formation. The electromagnetic parameters are measured using a vector network analyser in the microwave frequency range (*X* band, 8–12 GHz). Effects of composition thickness and input impedance with respect to matching frequency are studied. The presence of several reflection loss (RL) peaks at different frequencies is ruled by the impedance mechanisms and/or quarter wavelength mechanism. It is interesting to note that ferrite with $x = 0.4$ exhibits both mechanisms, and possesses a maximum RL peak of − 32.15 dB at a thickness of 1.6 mm. The other compositions, $x = 0.6, 0.8, 1.0$, have an absorption bandwidth of − 4.2 GHz spanning over the range 8.2 GHz to 12.4 GHz with − 10 dB wideband absorption. Further, ferrite with $x = 0.4$ shows an absorption band within 11.22–11.98 GHz with an absorption bandwidth of 0.76 GHz. This narrow band has an absorption strength of – 20 dB when the thickness $t = 1.7$ mm. In conclusion, absorption bandwidth, and hence microwave absorption, can be tuned by changing the thickness and composition of doped barium–strontium hexagonal ferrites, which can be used for various applications such as shielding, attenuation and fabrication of electromagnetic induction-based flexible absorbing sheets.

Keywords Hexagonal ferrite · ceramic method · magnetic properties · reflection loss · microwave absorption

Introduction

Nowadays, microwave absorbing materials are widely used in numerous applications, such as electromagnetic interference (EMI), electromagnetic compatibility (EMC) in commercial electronics and radar cross-section reduction (RCS) in the military.[1] These applications are due to the distinct property of absorption of EM waves by the material. Absorption of microwaves in these materials depends on the number of constraints, such as frequency response, impedance matching of absorbing material with free space, dielectric losses, magnetic losses and flexibility of the material over different series of frequencies. Arora et al.[2] studied the influence of La-Na doping on cobalt-titanium substituted barium hexaferrite for *X*-band microwave absorption. Ghasemi et al.[3] used doping of Mn, Co, and Zr in strontium ferrite and observed good reflection losses that are attained at a thickness of 1.6 mm by changing the substituted value of elements in strontium ferrite. Bierlich et al.[4] reported

✉ K. S. Bhatia
kamalbhatia.er@gmail.com

✉ A. Dhyani
adhyani@ddn.upes.ac.in

1 Department of Electronics and Communication Engineering, CTIEMT, Shahpur, Jalandhar, Punjab, India

2 Department of Electronics, G.B. Pant Institute of Engineering and Technology, Pauri Garhwal, Uttarakhand 246194, India

3 Department of Applied Sciences and Humanities, G.B. Pant Institute of Engineering and Technology, Pauri Garhwal, Uttarakhand 246194, India

4 Department of Applied Sciences, School of Engineering, University of Petroleum and Energy Studies, Dehradun, Uttarakhand 248007, India

single-phase *M*-type hexagonal ferrite $BaCo_xTi_xFe_{12-2x}O_{19}$. Their results show that coercivity and saturation magnetization decrease at room temperature with a decrease in substitution. Furthermore, they also reported an increase in permeability with Co/Ti substitution. Recently, Hussain et al.[5] studied $Zn_{1-x}Co_xGd_yFe_{2-y}O_4$ spinel ferrites to show a decrease in the lattice constant with an increase of Co and Gd content. In their study, they also observed an increase in remanence, coercivity and saturation magnetization. The complex permeability also increased with Co and Gd concentration although complex permittivity decreased. Jafarian et al.[6] reported a microwave absorber based on an amalgamation of hollow microspheres of iron carbonyl and polyaniline with mutli-walled carbon nanotubes (MWCNTs). Interestingly, they detected a major reflection loss of − 25.5 dB at 11 GHz with a bandwidth of 3.6 GHz and matching thickness of 2.0 mm. Pubbyet et al.[7] synthesized an *M*-type strontium hexaferrite to study the Co-Zr doping effect on the dielectric constant and loss tangent in a frequency range of 20 Hz to 120 MHz. Salman et al.[8] determined the optimum mole ratio for Fe/Ba in Ba-hexaferrite synthesized via mechanical activation. The absorption was reported in the *X*-band by using doping of Zr^{4+}, Sn^{4+}, Ti^{4+}. High saturation magnetization (49.80 emu/g) and a minimum reflection loss of − 29 dB at 12.2 GHz bandwidth are observed. Poorbafrani et al.[9] synthesized $Co_{0.6}Zn_{0.4}Fe_2O_4$ paraffin nanocomposites to find a resolution to the problem of the outdated spinal ferrite used as a microwave absorber. Their results show an improvement in saturation magnetization and coercivity with an increased reflection loss (23.6 dB) at 7.0 GHz. However, similar studies on various materials have shown different responses on microwave absorption. For example, thickness is inversely correlated to magnetic permeability, as reported in the references.[10–12] The barium hexaferrites (*M*-type or BaM hexaferrite), discovered more than six decades ago, have a wide range of technological and industrial applications.[13–15] Here, only a few suggested references are mentioned to highlight the progress in microwave absorption properties in doped hexaferrites.[16–20] In this work, we have reported microwave absorption of Co-In substituted Ba-Sr *M*-type ferrites with chemical composition $Ba_{0.5}Sr_{0.5}Co_xIn_xFe_{12-2x}O_{19}$ as a function of thickness and frequency. We have also discussed qualitatively the fundamental mechanisms behind the absorption.

Experimental Procedure

M-type hexagonal ferrites of composition $Ba_{0.5}Sr_{0.5}Co_xIn_xFe_{12-2x}O_{19}$ (x = 0.0, 0.2, 0.4, 0.6, 0.8, 1.0) are synthesized using the two-route standard ceramic method.[21] For sample preparation, high purity reagents such as barium carbonate ($BaCO_3$), strontium carbonate ($SrCO_3$), cobalt carbonate ($CoCO_3$), indium oxide (In_2O_3) and ferric oxide (Fe_2O_3) (from Sigma-Aldrich, 99.98% pure) are used. After the reactants have been weighed out in the requisite amounts, they are mixed collectively. The compounds are mixed in stoichiometric ratios to synthesize the ferrite series. An agate pestle and mortar (Model No SE-163) is used to crush the compound for 8 h using distilled water. After drying, pre-sintering is done at 1000°C for 10 h with slow heating and cooling rates of a proportional–integral–derivativ (PID) controller-based automatic electric furnace (Model No SE-130), set at +/− 5°C/min. The mixtures are then again ground to extremely fine powder under the identical situation. The sieving of sintered powders is carried out with sieves of B.S.S. mesh size 240. After that, polyvinyl alcohol is used as binder and aids homogenization in the filtered powder. The mixture is transformed into pellets using a hydraulic press under uniaxial pressure of 75 KN/m^2. Various pellets of size (10.16 mm × 22.86 mm) of varying thickness from 1.0 mm to 3.0 mm are sintered at 1100°C for final sintering for 15 h to analyse the modified microwave absorption properties of above samples sintered at 1150°C in our earlier work.[22] An electric furnace and the vector network analyzer (Agilent model N5225A) are used to measure microwave parameters associated with complex permittivity/permeability at the 8.2–12.4 GHz frequency range.

Results and Discussion

Electric and Magnetic Properties

To understand the absorption mechanism in $Ba_{0.5}Sr_{0.5}Co_xIn_xFe_{12-2x}O_{19}$, we have calculated electromagnetic parameters with varying frequencies. The parameters ε' and μ' represent the real part of the permittivity and permeability, respectively, signifying the storage of energy,[6–9,23,24] while ε'' and μ'' represent the imaginary parts of permittivity and permeability, respectively, signifying the inner dissipation ability for an incident electromagnetic wave. Figure 1 shows variation of ε' with doping concentration (x) and remains approximately constant after 10 GHz. However, frequency-dependent ε'' shows an increasing trend with increasing frequency initially and shows a decreasing trend relatively in a non-linear manner from 9.5 GHz to12.5 GHz.

The variation of permeability parameters (μ' and μ'') with frequency is also shown in Fig. 1. The μ' curve displays a large dispersion for x = 0.6, 0.8 and 1.0 for the studied frequency regime. However, undoped samples show non-linear variation. It is clearly evident from the figure that the doping causes a large decrease in μ' with respect to the undoped sample (x = 0.0). Further, the figure shows no significant change in μ' with frequency for the samples with x = 0.2 and 0.4. The parameter μ'' decreases

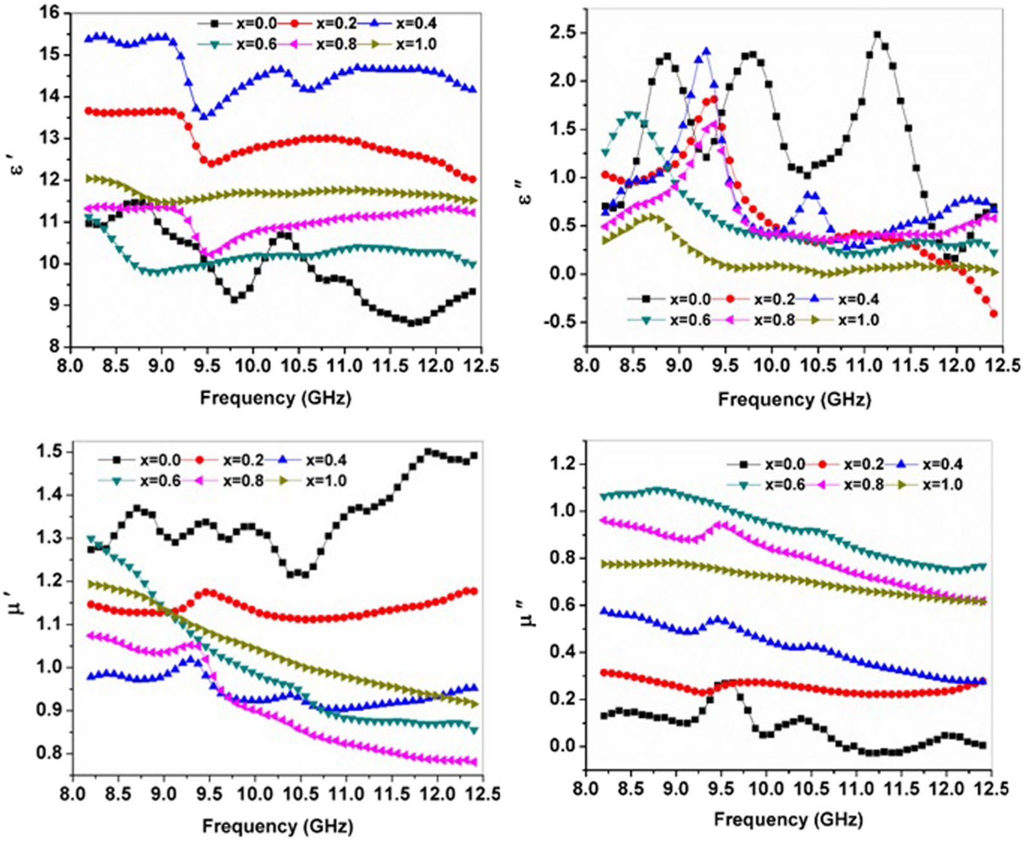

Fig. 1 Variation of electromagnetic parameters (ε', ε'', μ' and μ'') with frequency in doped *M*-type hexagonal ferrite $Ba_{0.5}Sr_{0.5}Co_xIn_xFe_{12-2x}O_{19}$ (© [2018] IEEE. Reprinted with permission, from Ref.23).

with an increase in frequency. It increases with doping from $x = 0.2$ to 0.6 and decreases thereafter with further doping.

Quarter Wavelength Mechanism

The quarter wavelength mechanism proves that when the thickness of ferrite material is equal to odd integer multiples of the wavelength ($n\lambda/4$, where $n = 1, 3, 5\ldots.$) of the microwave signal, the material will absorb or attenuate the signal when passing through the material.[25,26] Mathematically, this can be written as:

$$t_m = \frac{n.c}{4f_m\sqrt{|\mu_r\varepsilon_r|}} \tag{1}$$

where c = velocity of light, t_m = matching thickness, f_m = matching thickness, μ_r = complex permeability and ε_r = complex permittivity.

Rendering to transmission line theory, the reflection loss (RL) is related to the normalized input impedance (Z_{in}), which can be expressed as

$$RL = 20\log\left|\frac{Z_{in}-Z_o}{Z_{in}+Z_o}\right| \tag{2}$$

The impedance matching condition is given by $Z_{in} = Z_O$ to present perfect absorbing properties, where Z_{in} = input impedance of the metal back absorber and $Z_O = 377\ \Omega$ is the characteristic impedance. These are correlated as below:

$$Z_{in} = Z_O\sqrt{\frac{\mu_r}{\varepsilon_r}}\tanh\left[j\left(\frac{2\Pi ft}{c}\right)\sqrt{(\mu_r\varepsilon_r)}\right] \tag{3}$$

The microwave absorption properties are investigated for various In substituted ferrites (indium ion strength, $x = 0.0$, 0.2, 0.4, 0.6, 0.8 and 1.0) by plotting the reflection loss against frequency for simulated thickness. In Fig. 2, RL peaks are shown for $x = 0.0$ indium strength. It is observed that the maximum RL peak at thickness 1.9 mm, 2.0 mm, 2.1 mm is 9.54 GHz. The RL peak for 2.2 mm and 2.3 mm is 9.62 GHz. At thickness 2.4 mm, 2.5 mm, 2.6 mm, the RL peak is 9.71 GHz. In Fig. 2 it is also observed that RL peaks vary from − 10 dB to − 23.61 dB (for $x = 0.0$ composition) with more peaks in the lower frequency regime.

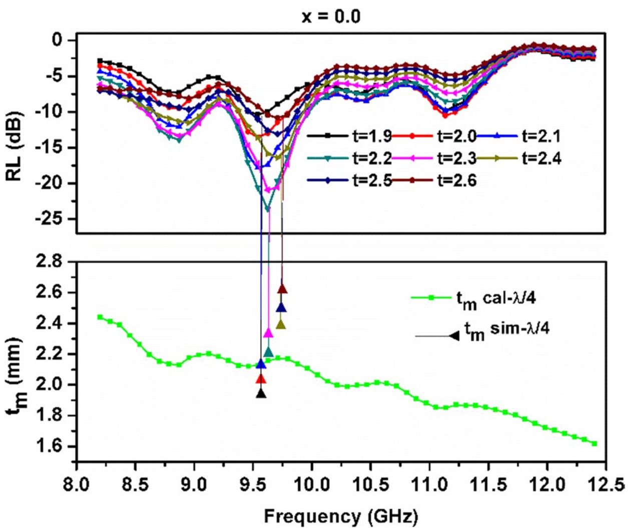

Fig. 2 Reflection loss (RL) versus frequency for simulated (t_m^{sim}) and calculated thickness (t_m^{cal}) in composition $x = 0.0$.

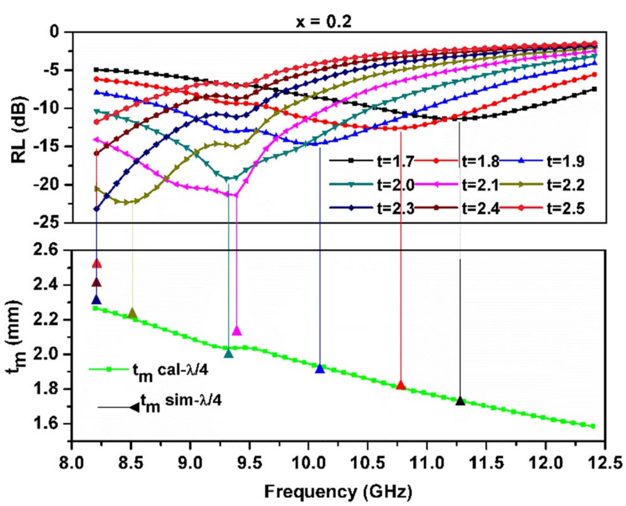

Fig. 3 Reflection loss (RL) versus frequency for simulated (t_m^{sim}) and calculated thickness (t_m^{cal}) in composition $x = 0.2$.

For the composition $x = 0.2$, RL peaks are observed at frequencies 8.4 GHz, 9.2 GHz, 9.3 GHz,10.04 GHz, 10.72 GHz and 11.14 GHz at a varying thickness of 2.2 mm, 2.0 mm, 2.1 mm, 1.9 mm, 1.8 mm, 1.7 mm, respectively, as shown in Fig. 3. These RL peaks are also observed as per quarter wavelength mechanism except at 2.1-mm thickness. For this particular case, the observed RL peak of − 21.35 dB appears at 9.37 GHz. For the composition of $x = 0.4$, the maximum RL is − 32.15 dB with a thickness of 1.6 mm. As frequency increases, thickness decreases which is presumably due to the quarter wavelength mechanism. Three RL peaks greater than – 20 dB are observed at 12.4 GHz, 11.64 GHz and 10.97 GHz against the simulated thickness of t

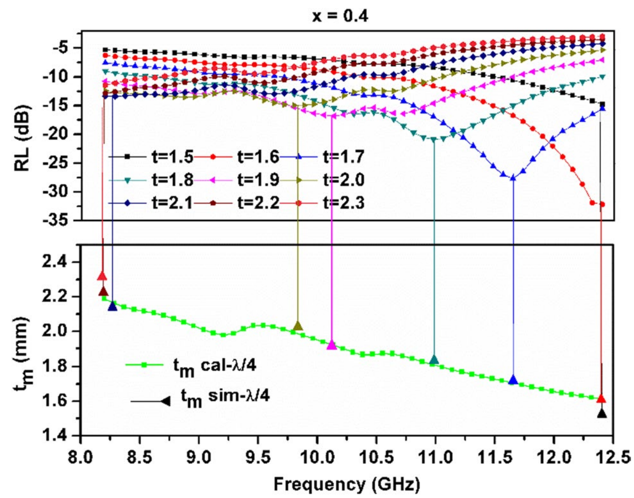

Fig. 4 Reflection loss (RL) versus frequency for simulated (t_m^{sim}) and calculated thickness (t_m^{cal}) in composition $x = 0.6$.

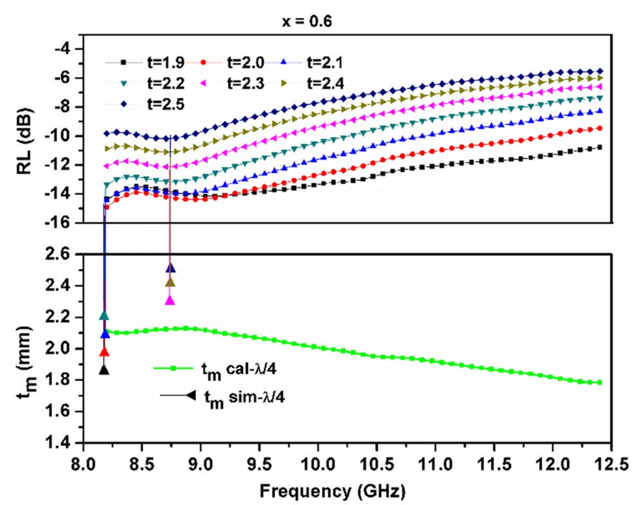

Fig. 5 Reflection loss (RL) versus frequency for simulated (t_m^{sim}) and calculated thickness (t_m^{cal}) in composition $x = 0.6$.

= 1.6 mm, 1.7 mm, 1.8 mm as shown in Fig. 4. There are no specified peaks for compositions $x = 0.6$, 0.8 and 1.0 as shown in Figs. 5, 6, 7.

The calculated thickness (t_m^{cal}) and simulated thickness (t_m^{sim}) are evaluated to verify the quarter wavelength mechanism as per the equations given above. t_m^{cal} is also plotted against the frequency for individual composition. For the composition of $x = 0.0$, Fig. 2 shows RL behaviour and variations of t_m^{cal} for different frequencies. To observe the close relationship between both thicknesses, i.e. simulated thickness and calculated thickness, we dropped the different colored lines from the RL peaks, which occurs in Fig. 2 to the response curve of calculated thickness and frequencies. Lower points of dropped lines are the simulated thicknesses

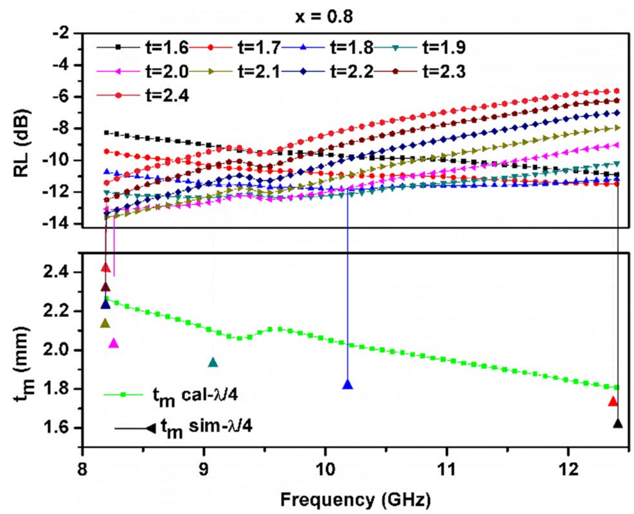

Fig. 6 Reflection loss (RL) versus frequency for simulated (t_m^{sim}) and calculated thickness (t_m^{cal}) in composition $x = 0.8$.

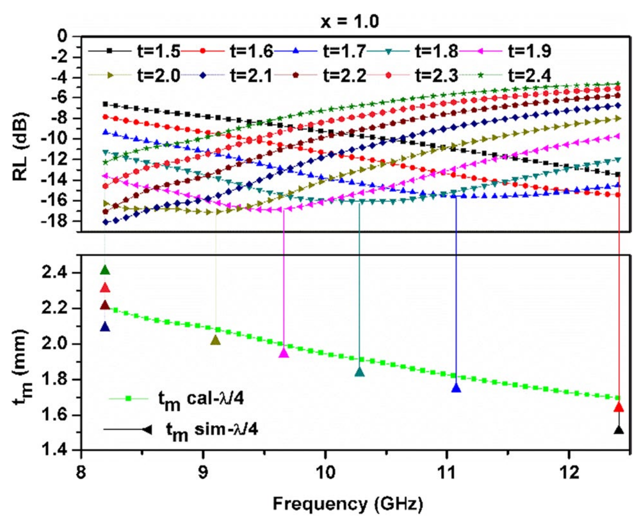

Fig. 7 Reflection loss (RL) versus frequency for simulated (t_m^{sim}) and calculated thickness (t_m^{cal}) in composition $x = 1.0$.

which are very close to the calculated thickness values. For $x = 0.0$, an RL value of − 23.61 dB occurs at frequency 9.62 GHz and a simulated thickness of 2.2 mm approximately matched their calculated thickness (2.156 mm) values and confirms the quarter wavelength mechanism. Calculated thickness was plotted against frequency for the quarter wavelength, i.e. for $n = 1$ as per Eq. 1.

Almost similar behavior was also observed for composition $x = 0.2$. In this case, RL of − 22.33 dB is observed at frequency 8.4 GHz and the simulated thickness of 2.2 mm exactly matches the calculated thickness value. At a frequency of 9.37 GHz, the RL of − 21.35 dB at $t = 2.1$ mm also shows a very close relationship between the simulated and calculated thickness values. Similarly, for the composition of $x = 0.4$, simulated thickness values are exactly the same as calculated thickness values for RL − 32.15 dB and − 27.67 at frequencies 12.4 GHz and 11.64 GHz, respectively.

RL of greater than − 10 dB in the narrow bandwidth region of 8.2 GHz to 12.4 GHz, finds use in a number of applications such as circulators, satellite downlinks, and junction isolators. Wide bandwidth is used for other applications such as radar, microstrip antenna and electromagnetic absorber panels.

Impedance Matching Mechanism

Figure 8 shows the various curves for RL and $|Z_{in}|$ with various values of frequency for materials with different Co and In compositions ($x = 0.0$, 0.2, 0.4, 0.6, 0.8 and 1.0) along with varying thickness values. As per Eq. 2, Reflection loss should be maximum or move towards infinity as Z_{in} approaches Z_o (377 Ω), i.e. characteristic impedance. For a better view, a line parallel to the x-axis is drawn at 377 Ω; if Z_{in} touches this line or is close to it, at this frequency RL should be maximum. This is referred to as impedance matching phenomenon. To analyse this relationship, we have plotted RL and Z_{in} with different values of frequency as shown in the figures.

Firstly, the graphs are plotted for composition $x = 0.0$ (Fig. 8) for different thickness values of $t = 2.2$ mm and 2.3 mm as these compositions have RL greater than − 20 dB which is very useful for the purpose of different microwave applications. Now we analyse the impedance matching criterion from the plotted graphs. It is observed that at lower RL values, Z_{in} is quite far away from Z_o (377 Ω), hence impedance matching is absent for the composition of $x = 0.0$. Similar behaviour is noticed for composition $x = 0.2$ at various thickness values of $t = 2.0$ and 2.1 mm as shown in Fig. 9. Quite good RL is observed for $x = 0.4$ composition for 1.6 mm thickness (Fig. 10). For this, when Z_{in} is very close to 377 Ω, i.e. Z_o, RL peak is present and it is quite close to Z_o (395 Ω).

For the compositions of $x = 0.6$, 0.8, 1.0 with thickness t = 2.0, 1.9 and 2.0, RL peaks (Figs. 11, 12, 13) are observed with Z_{in} away from Z_o (377 Ω) depicting that impedance matching is not satisfied with these concentrations.

This anomaly is associated with $|Z_{in}|$; as per Eq. 2, Z_{in} is a complex valued number, i.e. ($a + jb$), where a is real and b is imaginary. So Z_{in} can be written as $Z_{real} + j\,Z_{img}$. As discussed above, RL will be infinite as per Eq. 1 if $|Z_{in}| = Z_o = 377$ Ω, which means Z_{real} should be equal to 377 Ω and Z_{img} should be zero.[27–29] On the other hand, if Z_{real} moves away from 377 Ω and Z_{img} acquires positive or negative values other than zero, RL should acquire a finite value. Table I describes the analytical values for different

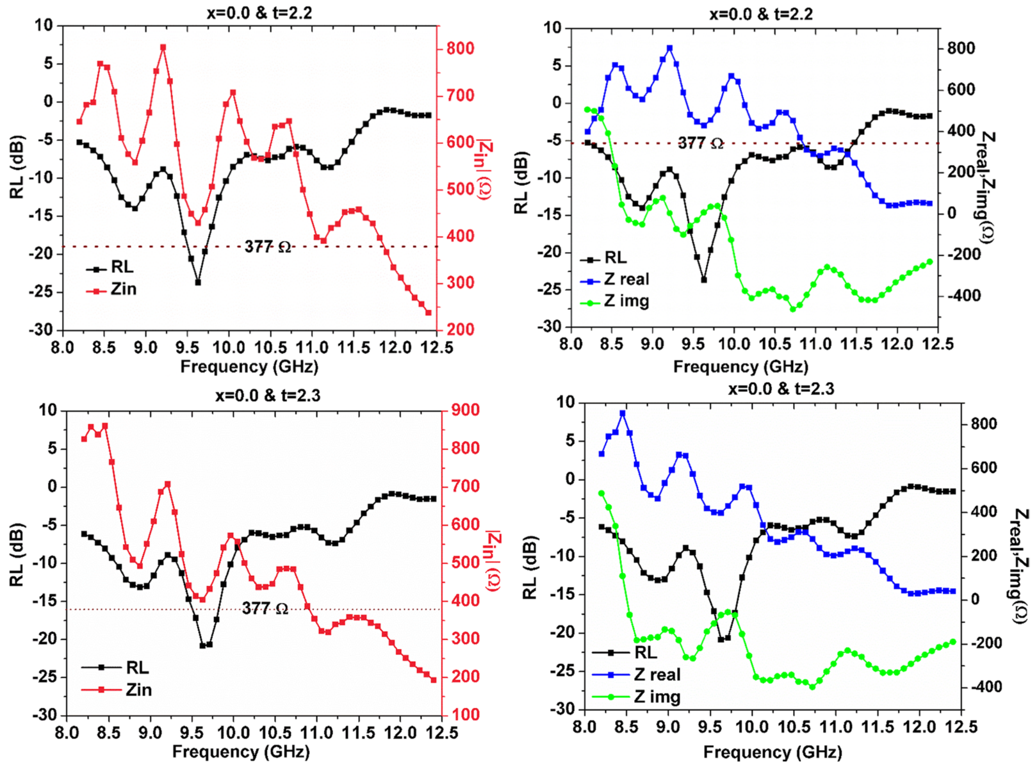

Fig. 8 Dependence of RL on Z_{in} and frequency for composition $x = 0.0$ at thickness 2.2 mm and 2.3 mm.

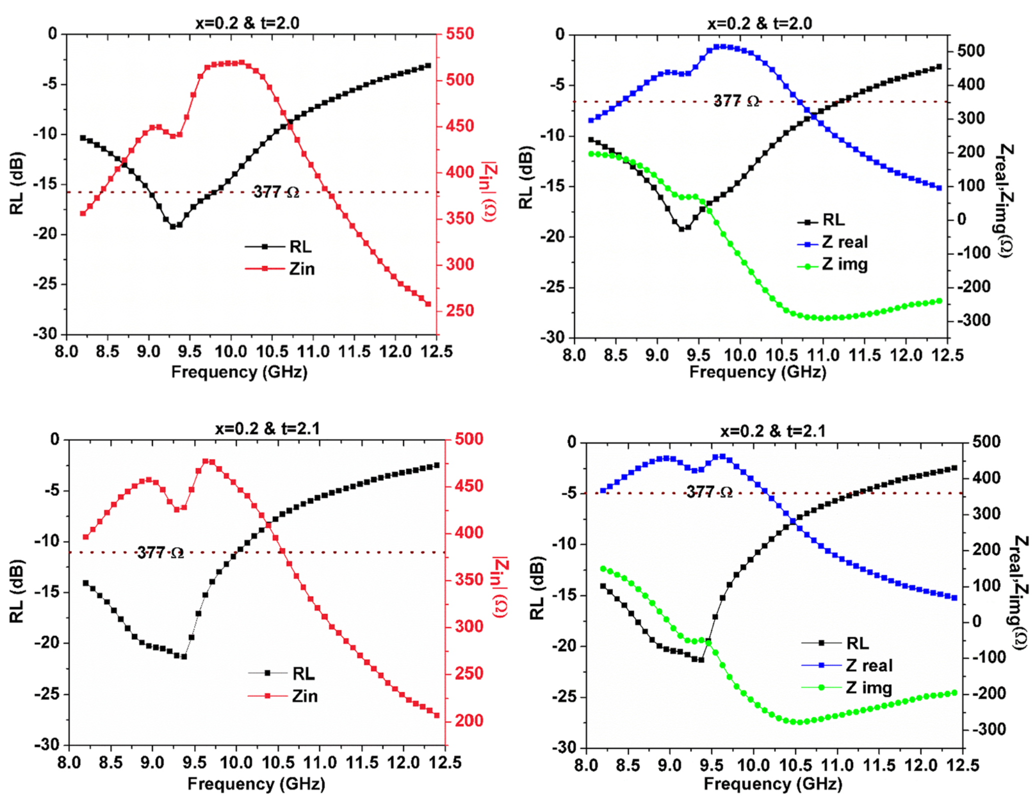

Fig. 9 Dependence of RL on Z_{in} and frequency for composition $x = 0.2$ at thickness 2.0 mm and 2.1 mm.

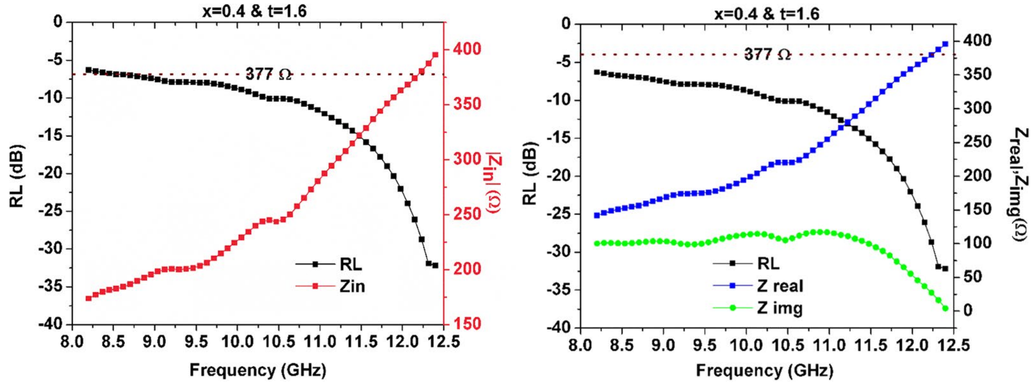

Fig. 10 Dependence of RL on Z_{in} and frequency for composition $x = 0.4$ at thickness 1.6 mm.

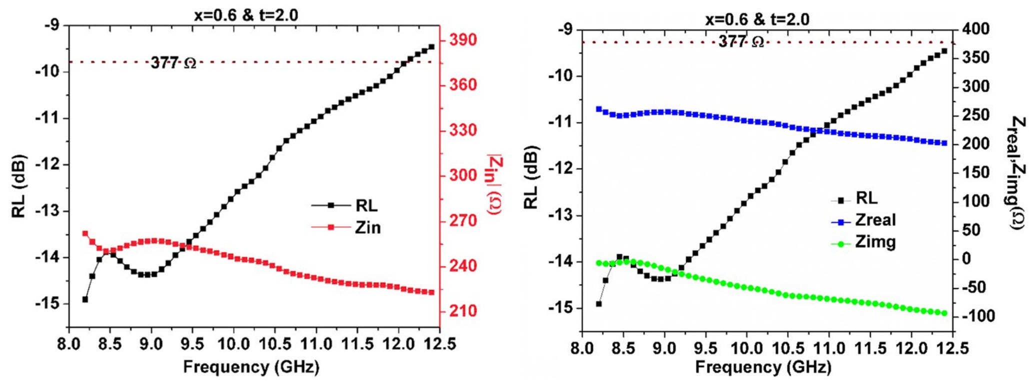

Fig. 11 Dependence of RL on Z_{in} and frequency for composition $x = 0.6$ at thickness 2.0 mm.

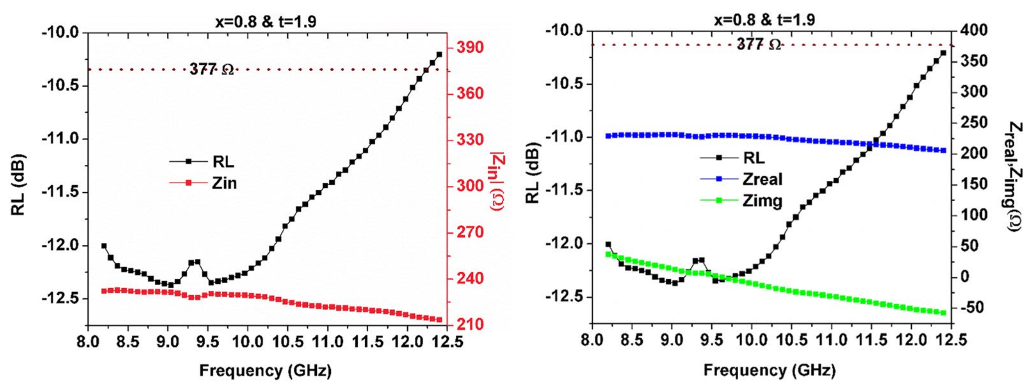

Fig. 12 Dependence of RL on Z_{in} and frequency for composition $x = 0.8$ at thickness 1.9 mm.

cases as discussed above. It clarifies the values of RL peaks (>− 10dB and > − 20dB) at their respective matching frequencies for different compositions, $x = 0.0$, 0.2, 0.4, 0.6, 0.8 and 1.0, at different thickness values. Further, frequency bands and bandwidths in the respective cases are also tabulated for easy guidance.

To confirm and examine the occurrence of reflection loss peaks in the absence of impedance matching, the figures of Z_{real} and Z_{img} are also plotted against matching frequency. This indicates Z_{real} and Z_{img} values conform to the extreme reflection loss peaks for diverse compositions of $x = 0.0$, 0.2, 0.4, 0.6, 0.8 and 1.0 at variable thickness values. The highest RL is − 32.15 dB in $x = 0.4$ with Z_{real} as 395 Ω and Z_{img} as 4.25 Ω at thickness $t = 1.6$ mm. For other compositions, $x = 0.0$, 0.6, 0.8 and 1.0, Z_{real} diverges from 377 Ω and Z_{img} from zero with more margin. Therefore, Z_{real} and Z_{img} values

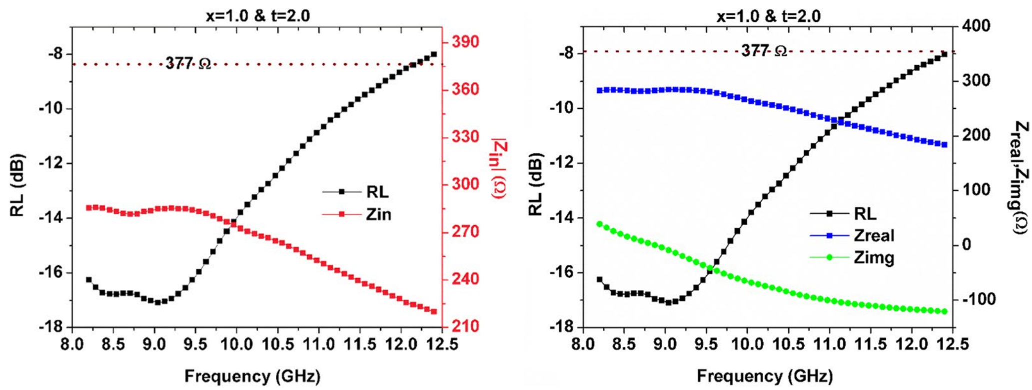

Fig. 13 Dependence of RL on Z_{in} and frequency for composition $x = 1.0$ at thickness 2.0 mm.

Table I Matching thickness, matching frequency, frequency band and bandwidth for RL ≥ − 10 dB and − 20 dB in $Ba_{0.5}Sr_{0.5}Co_xIn_xFe_{12-2x}O_{19}$ ($x = 0.0$, 0.2, 0.4, 0.6, 0.8 and 1.0) hexagonal ferrites

x	Max. RL (dB)	Matching thickness (mm)	Matching frequency (GHz)	Frequency band (GHz) for RL > − 10 dB	− 10 dB Absorption bandwidth (GHz)	Frequency band (GHz) for RL > − 20 dB	− 20 dB Absorption bandwidth (GHz)
0.0	− 23.61	2.2	9.62	8.62–9.04	0.42	9.54–9.62	0.08
				9.37–9.96	0.59		
	− 20.94	2.3	9.62	8.62–9.04	0.42	9.62–9.71	0.09
				9.37–9.96	0.59		
	− 17.82	2.1	9.54	8.70–8.95	0.25	–	–
				9.37–9.88	0.51	–	–
0.2	− 19.23	2.0	9.29	8.2–10.46	2.26	–	–
	− 21.35	2.1	9.37	8.2–10.13	1.93	8.95–9.37	0.42
	− 22.33	2.2	8.4	8.2–9.71	1.51	8.2–8.7	0.5
0.4	− 32.15	1.6	12.4	10.38–12.4	2.02	11.89–12.4	0.51
	− 27.67	1.7	11.64	9.71–12.4	2.69	11.22–11.98	0.76
	− 20.86	1.8	10.97	8.6–12.31	3.71	10.88–11.05	0.17
0.6	− 13.31	1.8	9.37	8.2–12.4	4.2	–	–
	− 14.35	1.9	8.2	8.2–12.4	4.2	–	–
	− 14.90	2.0	8.2	8.2–11.89	3.69	–	–
0.8	− 12.37	1.9	9.04	8.2–12.4	4.2	–	–
	− 13.10	2.0	8.28	8.2–11.56	3.36	–	–
	− 13.56	2.1	8.2	8.2–10.72	2.52	–	–
1.0	− 16.04	1.8	10.38	8.2–12.4	4.2	–	–
	− 16.87	1.9	9.54	8.2–12.3	4.1	–	–
	− 17.09	2.0	9.04	8.2–11.30	3.1	–	–

in $x = 0.0$, 0.6, 0.8, 1.0 are suggestive of less involvement of the impedance mechanism.

As discussed, the quarter wavelength criterion also occurs in $x = 0.0$, 0.2 and 0.4 for extreme RL peaks at the similar thickness and matching frequencies. Therefore, both the quarter wavelength mechanism and an impedance mechanism are satisfied with the composition $x = 0.4$. The substitution of indium ions widens absorption followed by RL of − 32.15 dB in $x = 0.4$ and shifts the RL peaks to low frequencies.

Conclusions

We conclude that microwave absorption can be enhanced by Co-In doping in M-plane ferrites that depends on sintering temperature. Optimum concentration ($x = 0.4$) satisfies both mechanisms, quarter wavelength and impedance matching, giving maximum RL peaks with an absorption of ~ − 32.15 dB. It is observed that the compositions $x = 0.2$ and 0.4 have more contribution to quarter wavelength. Absorption is suppressed for other compositions, such as $x = 0.6$, 0.8 and 1.0, showing an absorption of ~ − 10 dB. Wideband absorption is achieved at 4.2 GHz with absorption bandwidths of 8.2 GHz to 12.4 GHz at 1.8 mm and 1.9 mm. Also, there exists narrowband absorption (0.76 GHz) with bandwidths from 11.22 GHz to 11.98 GHz with absorption strength of ~ − 20 dB for $x = 0.4$ and $t = 1.7$ mm. Our studies show tunable microwave absorption characteristics in indium-doped *M*-plane hexagonal ferrites by simply varying thickness of the material layer and wide range of dopant concentration.

Conflict of interest The authors declare that they have no conflict of interest.

References

1. T. Giaimakopoulou, A. Oikonomou, and G. Kordas, Double-Layer Microwave Absorbers Based on Materials with Large Magnetic and Dielectric Losses. *J. Magn. Magn. Mater.* 271, 33 (2004).
2. A. Arora and S. Bindra, Effect of La-Na Doping in Co-Ti Substituted Barium Hexaferrite on Electrical and X-Band Microwave Absorption Properties. *J. Electron. Mater.* 47, 4919 (2018).
3. A. Ghasemi and A. Morisako, Structural and Electromagnetic Characterstics of Substituted Strontium Hexaferrites Nanoparticles. *J. Magn. Magn. Mater.* 320, 1167 (2008).
4. S. Bierlich, T. Reimann, H. Bartsch, and J. Töpfer, Co/Ti-Substituted M-Type Hexagonal Ferrites for High-Frequency Multilayer Inductors. *J. Magn. Magn. Mater.* 384, 1 (2015).
5. M. Hussain, M. Islam, T. Meydan, J.A. Cuenc, Y. Melikhov, G. Mustafa, G. Murtaza, and Y. Jamil, Microwave Absorption Properties of CoGd Substituted $ZnFe_2O_4$ Ferrites Synthesized by Co-precipitation Technique. *Ceram. Int.* 44, 5909 (2018).
6. M. Jafarian, S.S.S. Afghahi, Y. Atassi, and M. Salehi, Enhanced Microwave Absorption Characteristics of Nanocomposite Based on Hollow Carbonyl Iron Microspheres and Polyaniline Decorated with MWCNTs. *J. Magn. Magn. Mater.* 462, 153 (2018).
7. K. Pubby, S.K. Chawla, P. Kaur, G. Kaur, and S.B. Narang, Effect of Precursors on Dielectric Properties of Co-Zr Doped Strontium Hexaferrites in 20 Hz–120 MHz Frequency Range. *Ferroelectrics* 505, 67 (2016).
8. S. Salman, S. Afghahi, M. Jafarian, M. Salehi, and Y. Atassi, Improvement of the Performance of Microwave X Band Absorbers Based on Pure and Doped Ba-Hexaferrite. *J. Magn. Magn. Mater.* 421340, 348 (2017).
9. A. Poorbafrani and E. Kiani, Enhanced Microwave Absorption Properties in Cobalt–Zinc Ferrite Based Nanocomposites. *J. Magn. Magn. Mater.* 416, 10 (2016).
10. A. Arora, S.B. Narangb, and K. Pubby, Effect of Thickness on Microwave Absorptive Behavior of La-Na Doped Co-Zr Barium Hexaferrites in 18.0–26.5 GHz Band. *J. Magn. Magn. Mater.* 423, 441 (2017).
11. X.-M.L.-Y. Hong-Mei Xiao, Synthesis, Magnetic and Microwave Absorbing Properties of Core-Shell Structure $MnFe_2O_3/TiO_2$ Nanocomposite. *Compos. Sci. Technol.* 66, 2003 (2006).
12. W.P. Li, L.Q. Zhu, J. Gu, and H.C. Liu, Microwave Absorption Properties of Fabric Coated Absorbing Materials Using Modified Carbonyl Iron Powder. *Compos. Part B Eng.* 42, 626 (2011).
13. F.Q. Brosseau, A Review and Analysis of Microwave Absorption in Polymer Composite Filled with Carbonaceous Particles. *J. Appl. Phys.* 111, 061301 (2012).
14. R.C. Pullar, Hexagonal Ferrites: A Review of the Synthesis, Properties and Applications of Hexaferrite Ceramics. *Prog. Mater Sci.* 57, 1191 (2012).
15. U. Ozgur, Y. Alivov, and H. Morkoc, Microwave Ferrites, Part 1: Fundamental Properties. *J. Mater. Sci. Mater. Electron.* 20, 789 (2009).
16. H.H. Nguyen, N. Tran, T.L. Phan, D.S. Yang, N.T. Dang, and B.W. Lee, Electronic Structure and Magnetic and Microwave Absorption Properties of Co-Doped $SrFe_{12}O_{19}$ Hexaferrites. *Ceram. Int.* 46, 19506 (2020).
17. S. Gupta, S.K. Deshpande, V.G. Sathe, and V. Siruguri, Effect of Scandium Substitution on Magnetic and Transport Properties of the M-Type Barium Hexaferrites. *J. Alloys Compd.* 815, 152467 (2020).
18. S. Goel, A. Garg, R.K. Gupta, A. Dubey, N.E. Prasad, and S. Tyagi, Effect of Neodymium Doping on Microwave Absorption Property of Barium hexaferrite in X-Band. *Mater. Res. Exp.* 7, 1 (2020).
19. H. Sözeri, F. Genç, M.A. Almessiere, Ä.S. Ünver, A.D. Korkmaz, and A. Baykal, Cr^{3+} -Substituted Ba Nanohexaferrites as High-Quality Microwave Absorber in X Band. *J. Alloys Compd.* 779, 420 (2019).
20. G. Gultom, M. Rianna, P. Sebayang, and M. Ginting, The Effect of Mg–Al Binary Doped Barium Hexaferrite for Enhanced Microwave Absorption Performance. *Case Stud. Thermal Eng.* 18, 100580 (2020).
21. C. Singh, S.B. Narang, I.S. Hudiara, K. Sudheendran, and K.C. James Raju, Complex Permittivity and Complex Permeability of Sr Ions Substituted Ba Ferrite at X-Band. *J. Magn. Magn. Mater.* 320, 1657 (2008).
22. H. Kaur, A. Marwaha, C. Singh, S. Narang, R. Jotania, Y. Bai, S.R. Mishra, D. Singh, A.S.B. Sombra, M. Ghimire, and P. Dhruv, Tailoring of Electromagnetic Absorption in Substituted Hexaferrites from 8.2 GHz to 12.4 GHz. *J. Electron. Mater.* 49, 1646 (2020).
23. H. Kaur, C. Singh, A. Marwaha, Qualitative analysis of microwave absorption for Indium doped M-type hexagonal ferrite ($Ba_{0.5}Sr_{0.5}Co_xIn_xFe_{12-2x}O_{19}$) in X- band, in *International Conference on Intelligent Circuits and Systems Proceedings* (2018), p. 224
24. C.-C. Huang, C.-C. Mo, T.-H. Hsiao, Z.-B. Li, and H.-H. Hsu, Preparation and Magnetic Properties of Lanthanum- and Cobalt-Substituted M-type Sr Base Sintered Magnets. *Jpn. J. Appl. Phys.* 60, 115504 (2021).
25. M. Jamalian, A. Ghasemi, and E. Paimozd, A Comparison of the Magnetic and Microwave Absorption Properties of Mn-Sn-Ti Substituted Strontium Ferrite With and Without Multi-walled Carbon Nanotube. *Curr. Appl. Phys.* 14, 909 (2014).
26. H. Peng, M. Fan, and Z. He, A Method for Analyzing the Microwave Absorption Properties of Magnetic Materials. *J. Magn. Magn. Mater.* 324, 2492 (2012).
27. S. Gujral, K.S. Bhatia, H. Singh, H. Kaur, and N. Gupta, Microwave Absorption Properties of Co-La Doped M-type Ba-Sr Hexagonal Ferrites in X-Band. *J. Optoelectron. Adv. Mater.* 23, 397 (2021).
28. S. Gujral, K.S. Bhatia, H. Singh, H. Kaur, and N. Gupta, Investigations on Structural and Magnetic Properties of M-Type Hexagonal Ferrite $Ba_{0.5}Sr_{0.5}CoxLaxFe_{12-2x}O_{19}$ in X-Band. *J. Mater. Sci. Mater. Electron.* 32, 1 (2021).
29. M. Rani, K.S. Bhatia, H. Singh, H. Kaur, and N. Gupta, Synthesis of Suitable Material for Microwave Absorbing Properties in X-Band. *SN Appl. Sci.* 2, 2035 (2020).